Genome-wide DNA Methylation Patterns in *Daphnia magna* are Not Significantly Associated with Age

Authors

Ruoshui Liu[1], Marco Morselli[2], Lev Y. Yampolsky[3], Leonid Peshkin*[4], Matteo Pellegrini*[1]

[1] Department of Molecular, Cell and Developmental Biology, University of California, Los Angeles, CA 90024, USA

[2] Department of Chemistry, Life Sciences, and Environmental Sustainability, University of Parma, Parma, Italy

[3] Department of Biological Sciences, East Tennessee State University, Johnson City, TN 37614, USA

[4] Systems Biology, Harvard Medical School, Boston, MA 02115, USA

* Corresponding Authors

pesha@hms.harvard.edu

matteop@ucla.edu

Abstract

Studying DNA methylation in *Daphnia magna*, a model organism in ecological and evolutionary research, offers valuable insights into pharmaceutical toxicity and behavioral ethology. In this study, we characterized DNA methyltransferases and mapped DNA methylation across the *D. magna* genome using whole-genome bisulfite sequencing. Our analysis revealed a highly expressed, nonfunctional *de novo* methyltransferase (DNMT3.1) alongside lowly expressed functional *de novo* methyltransferase DNMT3.2 and maintenance methyltransferase DNMT1. *D. magna* displays overall low DNA methylation, targeting primarily CpG dinucleotides. Methylation is sparse at promoters but elevated in the first exons downstream of transcription start sites, with these exons showing hypermethylation relative to adjacent introns. In contrast to prior studies, we observed minimal age-related changes in DNA methylation patterns that were not sufficiently robust to build an accurate epigenetic clock. These findings expand our understanding of the epigenetic landscape in *D. magna*.

Keywords

Daphnia magna; DNA methylation; epigenetic clock; DNA methyltransferase (DNMT)

INTRODUCTION

Daphnia are planktonic crustaceans within the Phyllopoda subclass and the Branchiopoda class (1). Among over 100 species within the *Daphnia* genus, *Daphnia magna* (*D. magna*) is widely recognized as a model organism in biological research, including studies on pharmaceutical toxicity, reproductive cycles, behavioral ethology, and phenotypic plasticity (2). DNA methylation, the addition of a methyl group on the 5' carbon of cytosine, plays a role in transcriptional regulation and phenotypic expression (3). Previous studies have demonstrated that DNA methylation assessment aids in toxicity evaluation (4). Given the significance of *D. magna* as a model organism, examining its epigenomics landscape, particularly DNA methylation pattern and regulation, could be critical (5).

CpG methylation is closely associated with gene silencing and is crucial for development (6,7). In *Daphnia magna*, cytosine methylation levels are relatively low, yet specific regions, such as exons, exhibit higher methylation (3,6,8). Previous studies, however, have tended to average methylation across different genes for each exon, overlooking the nuanced methylation patterns of individual genes and exons. To address this gap, our study aims to examine both average methylation patterns and detailed variations at the exon and gene levels across different genes.

DNA methyltransferases (DNMTs) are a family of enzymes that epigenetically regulate gene expression by establishing and maintaining CpG methylation patterns (9). Maintenance methyltransferase DNMT1 replicates DNA methylation patterns to daughter cells during cell divisions, while the functional *de novo* methyltransferase DNMT 3 establishes methyl groups at unmethylated cytosine sites (10,11). Our research aims to explore the functional domains of *D. magna*'s DNMTs and their effect on genome-wide and gene-specific methylation patterns.

DNA methylation levels vary with age and influence the functional capability of organs in mammals, positioning DNA methylation-based biomarkers, also known as epigenetic clocks, as effective estimators of biological age (12–14). Epigenetic clocks facilitate understanding the impact of both endogenous (epigenetic drift, etc.) and exogenous stressors on biological aging by comparing epigenetic age to chronological age (12,14). In a previous study, an epigenetic clock for *D. magna* was built with 12 clock CpGs (6). However, this analysis was conducted using samples from only two age groups: 10-day and 50-day-old. Additionally, they incorporated *Daphnia* specimens from two different strains and included an interaction term for strain and age in their epigenetic clock. Both the large age gaps and an additional factor of strain potentially diminished the predictive accuracy of their regression model (6). Thus, further research is needed to characterize age-related changes in DNA methylation and determine the validity of an epigenetic clock for *D. magna*.

64 This study aimed to investigate the targeting and age association of DNA methylation in *D.*
65 *magna*. We cultured 17 *D. magna* samples of various ages, performed whole genome bisulfite
66 sequencing, and characterized the DNA methylation patterns at the genome-wide, gene, and exon levels.
67 To better understand the methylation patterns, we analyzed functional domains and mRNA expression
68 levels of DNA methyltransferases. Lastly, we examined age-related changes in methylation patterns and
69 attempted to build an epigenetic clock.
70

MATERIALS AND METHODS

Sample collection

A heat-tolerant clone of D. magna, IL-MI-8, was originally acquired from the Ebert Lab at the University of Basel, Switzerland. This clone was sourced from a pond in Jerusalem, Israel, as part of the Ebert Lab stock collection. To ensure synchronized cohorts, neonates born within a two-day window were separated from their mothers. Sex was determined at 8- to 9-day-old animals. Female individuals were exclusively used in all experiments conducted in this study. All mothers received adequate nutrition and were cultured under identical conditions at 25°C within an incubator. All cultures, including mother cultures, neonate cultures, and tank cultures, were maintained in ADaM water (15). Animals were exposed to a light cycle consisting of 16 hours of light followed by 8 hours of darkness. Animals were fed a daily suspension of the green alga Scenedesmus obliquus at a concentration of 10^5 cells/ml (adjusted for population density, with one animal per 20 ml). Every sixth day, the water was replaced, and offspring were manually removed until animals were transferred to the culture platform. The operational protocols for the culture platform are akin to those described in previously published protocols (16).

DNA extraction and WGBS library preparation

Approximately 30-50 ng of purified genomic DNA in 50 µl has been subject to sonication using the Bioruptor Pico (Diagenode) for 15 cycles (30 ON; 90 OFF). Fragmentation patterns have been checked with the D1000HS Assay (Agilent Technologies) on a 4200 TapeStation. The volume of the fragmented DNA has been reduced to 20 µl using a Vacufuge (Eppendorf), then subject to bisulfite conversion using the EZ DNA Methylation-Lightning Kit (Zymo Research). The libraries have been prepared using the Accel-NGS Methyl kit (Swift Biosciences - now xGen Methyl-Seq Library Prep - IDT) according to the manufacturer's recommendations except for a major modification. Briefly, the denatured BS-converted gDNA was subject to the adaptase, extension, and ligation reaction. Following the ligation purification, the DNA underwent primer extension (98C for 1 minute; 70C for 2 minutes; 65C for 5 minutes; 4C hold) using oligos containing random UMI at the location of the i5 barcode. The extension using a UMI-containing primer allows the tagging of each molecule to remove PCR duplicates and correctly estimate DNA methylation levels. Following exonuclease I treatment and subsequent purification, the libraries were then amplified using a universal custom P5 primer and i7-barcoded P7 primers (initial denaturation: 98C for 30 seconds; 10 cycles of 98C for 10 seconds, 60C for 30 seconds, 68C for 60 seconds; final extension: 68C for 5 minutes; 4C hold). The resulting single-indexed libraries were then purified and quantified using the Qubit HS-dsDNA assay, and the quality was checked using

103 the D1000-HS assay (Agilent - TapeStation 4200). The libraries were sequenced as 150 PE on the
104 Illumina NovaSeq6000 platform.
105
106 **Bisulfite sequencing data processing**
107 An alignment index incorporating a bisulfite-converted sequence for each reference strand was
108 constructed from the *Daphnia magna* Xinb3 reference genome (BioProject ID: PRJNA624896, D. Ebert,
109 personal communication) and the mitochondrial genome (17), using the *BSBolt Index* tool v1.6.0 (18).
110 The FASTQ files were aligned using *BSBolt Align* (default options) (18). PCR duplicates were removed
111 with *samtools markdup* v1.17 (option -r) (19). Sequence alignment quality was assessed using the CIGAR
112 (compact idiosyncratic gapped alignment report) strings, and sequences with a total number of matches
113 below 50 were excluded from further analysis using *samtools view* and *samtools index* (19). The number
114 of mapped reads in each sample was quantified using *samtools flagstat* (19).
115 DNA methylation calling was performed with *BSBolt CallMethylation* (options: -IO) with the
116 DNA alignment index as a reference, generating CGmap files (18,20). The CGmap files were
117 subsequently filtered based on contig coverage and quality. Average coverage before and after filtering
118 for cytosines across each chromosome was obtained using *CGmaptools mec* v0.1.2 (20). Global DNA
119 methylation levels were analyzed with *CGmaptools mstat* (20), and differences in global methylation
120 levels of CpG and non-CpG cytosines were assessed using the Wilcoxon test. DNA methylation levels of
121 genes, exons, and introns were calculated using *CGmaptools mtr* (20). Metagene plots for genes and
122 exons were generated using *CGmaptools bed2fragreg* and *CGmaptools mfg* (20). Pathway enrichment
123 analysis was performed using the R package *clusterProfiler* (21). Genome browser snapshots were taken
124 from Integrative Genomics Viewer (version IGV_2.18.2) (22).
125 The matrix of common CpG sites was generated using *BSBolt AggregateMatrix* function (options:
126 -min-coverage 10 -min-sample 0.8 -CG) (18). To handle missing data, CpG sites absent in some samples
127 were imputed using the *BSBolt Impute* feature. UMAP was employed to visualize the clustering of
128 samples based on methylated CpG sites. This approach allowed us to examine whether *Daphnia* samples
129 from the same age group exhibited consistent methylation patterns, with an expectation of tighter
130 clustering within age groups in the UMAP plot (23).
131 The CpG sites were filtered to only include the ones with the top 20% of the variability. The
132 epigenetic clock model was built with the Lasso function from the Python module *sklearn.linear_model*
133 and Leave-One-Out Cross Validation (24). Differentially methylated regions (DMR) analysis was
134 performed using the *Metilene* package v0.2-8 (options: -m 10 -d 0.001 -t 4 -f 1) (25).

135 Random permutation was used to assess the statistical significance of differences in methylation
136 levels between age groups at each position within the meta-gene ridge plot. For each position, we
137 calculated the differences in mean methylation levels between the two age groups. We conducted 100,000
138 random permutations and reassigned sample labels to form two new groups, ensuring that the size of these
139 groups matched the age groups. In each permutation, we calculated the mean methylation difference
140 between these newly assigned groups. p-values were calculated as the proportion of permuted differences
141 as extreme as, or more extreme than, the observed differences, applying a two-tailed test. Significance at
142 each site was defined as p-value < 0.05. This procedure was utilized across three comparisons: mature
143 versus young, old versus young, and old versus mature.
144
145 **RNA sequencing data processing**
146 Details of an age-specific RNAseq experiment are reported elsewhere (26). Briefly, RNA was
147 extracted from somatic tissues (whole bodies) of *Daphnia magna* females from laboratory clone GB-
148 EL75-69 (Basel University *Daphnia* Stock Collection, Switzerland) of different ages: young, reproducing
149 (age 15-20 days), old, reproductively senescent, and old, reproductively rejuvenated (age both 130-175
150 days), in 4 replicates each. In all cases**,** *Daphnia* samples were sampled within 24 hours of molting and
151 egg-laying and freshly laid eggs (if any) were removed from the brood chamber before homogenizing
152 *Daphnia*. RNAs were extracted using Qiagen RNeasyPlus Mini kit and RNA library preparation was
153 performed using NEBNext Ultra II DirecMonal RNA Library Prep Kit (NEB, Lynn, MA) following the
154 manufacturer's protocols. The libraries were sequenced with Illumina Novoseq 6000, S4 flow cell, PE100.
155 Reads were mapped to *D. magna* Xinb3 reference transcriptome (BioProject ID: PRJNA624896; D. Ebert
156 and P. Fields, personal communication), and genes with differential expression between young vs. old
157 *Daphnia* were identified using DEseq2 (27). Statistical analysis of RNA expression levels between groups
158 was performed using a two-sided t-test.
159
160 **DNA methyltransferase analysis**
161 The functional analysis of DNMT3.1, DNMT3.2, DNMT1, and UHRF1 was conducted using
162 InterProScan (28). Gene sequences were input into the tool to identify and characterize the functional
163 domains within these methyltransferases. Nuclear localization signals were predicted using NLStradamus,
164 a Hidden Markov Model (HMM) tool, to assess their potential nuclear targeting (29). The analysis was
165 conducted using a 2-state HMM static model, and NLS sequences were identified based on a consensus
166 between the Viterbi path and posterior probability estimates exceeding 70%.

RESULTS

D. magna has three DNA methyltransferases

Based on the homology with other organisms' DNA methyltransferases (DNMTs), *D. magna* harbors two functional and one non-functional DNMT (**Table S1**) (9). It has two *de novo* DNMTs, *Dma*DNMT3.1 and *Dma*DNMT 3.2 (**Figure 1A**) (10).

To better understand DmaDNMT and its relationship with the species' methylation pattern, we used mammalian (human) DNMTs as a reference and compared the homologies between *Dma*DNMTs and *Hs*DNMTs. Mammalian DNMT3a/b contains a Pro-Trp-Trp-Pro (PWWP) domain, an ATRX-DNMT3A-DNMT3L (ADD) domain, and a DNA-(cytosine-C5)-Methyltransferase (MTase) domain with 6 motifs (I to VI). Non-functional *Dma*DNMT3.1 is missing 5 critical motifs in the MTase domain, and it is thought to exert similar functions to mammalian DNMT3L. Both *Dma*DNMT3.1 and *Hs*DNMT3L contain putatively functional ADD domains that do not bind H3K4me3. However, *Dma*DNMT3.1 owns the PWWP domain that is known to bind methylated lysines, specifically H3K36me2/3 in mammals (11).

Conversely, the functional *de novo* DNA methyltransferase, *Dma*DNMT3.2, contains all six DNA methyltransferase motifs and the ADD domain, suggesting that it can sense the methylation status of H3K4 and bind unmethylated H3K4 histones (10). However, it is missing the N-terminal PWWP domain present in the active mammalian DNMT3A and DNMT3B.

The other putatively active DNA methyltransferase in *D. magna* is the maintenance methyltransferase *Dma*DNMT1 (**Figure 1A**). Compared to the mammalian counterpart, *Hs*DNMT1, it is missing the N-terminal domains involved in the targeting of the replication foci, including the DNA methyltransferase 1-associated protein-binding domain (DMAP1-BD) and the proliferating cell nuclear antigen-binding domain (PCNA-BD). NLStradamus predicted *Dma*DNMT1's nuclear localization signals (NLS) both upstream (position 403-434) and downstream (678-696) of the DRFtD domain, with the upstream NLS aligning with the conserved position in *Hs*DNMT1. Additionally, a phosphatase-specific domain (PAP2-wunen) at the N-terminal region is unique to *Dma*DNMT1.

To understand the activity of the three *Dma*DNMTs, we analyzed RNA sequencing data across two age groups: young and old (**Figure 1B**). Gene expression levels (TPM) varied significantly across the three *Dma*DNMTs by a two-sided t-test. The two functional enzymes, *Dma*DNMT1 and *Dma*DNMT3.2, exhibited consistently low expression levels with no significant differences between the age groups. By contrast, the non-functional *Dma*DNMT3.1 showed significantly higher expression in the old group compared to the young group. However, since *Dma*DNMT3.1 lacks the critical DNA methyltransferase motifs, its expression is unlikely to impact methylation levels.

199 **High-coverage *D. magna* Methylomes**

200 To determine the DNA methylation profiles of *Daphnia magna*, we obtained two 45-day-old
201 (mature-old) Xinb3 clone individuals, Dap_S1 and Dap_S2. Whole-genome bisulfite sequencing was
202 performed as described in Materials and Methods, and subsequent sequence alignment to the *D. magna*
203 genome and methylation calling was carried out. On average, approximately 79% of the reads mapped
204 primarily to the genome, and this dropped to 56% after removing duplicates and 53% after filtering by
205 CIGAR (compact idiosyncratic gapped alignment report) strings. The *Daphnia magna* genome comprises
206 56.6 million cytosine sites across both strands. Applying a minimum coverage threshold of 10 reads per
207 site in the methylation calling step, we successfully identified 41.1 million cytosines, representing
208 approximately 72.6% of the total cytosine sites in the genome. Although the average coverage across
209 contigs was around 60, the distribution demonstrated large variations (**Figure S1A**).

210 The original genome assembly of *Daphnia magna* consisted of one mitochondrial genome (17)
211 and 608 nuclear contigs (BioProject ID: PRJNA624896, D. Ebert, personal communication), many of
212 which are short. Approximately 50% of these contigs are under 20,000 base pairs and 25% are below
213 10,000 base pairs in length. Some short contigs showed pronounced high coverage and hypermethylation
214 at CpG sites, suggesting that they are outliers and possible contaminants. To improve the quality of
215 methylome, alignment filtration was implemented, retaining only the CpN sites from the top-performing
216 97 nuclear contigs validated by genetic recombination map, Hi-C data, and optical mapping (BioProject
217 ID: PRJNA624896, D. Ebert, personal communication). Following selective filtration, 38.7 millions of
218 these 41.1 million covered cytosine sites (94.1%) were retained for each sample. The mean contig length
219 was 1.3 million base pairs, with an average coverage of approximately 60x (**Figure S1B**). This process
220 reduced variability across contigs and confirmed the reliability of the remaining methylcytosine sites.
221 Consequently, the cytosine sites chosen for our downstream analysis were situated on the top-performing
222 contigs with a minimum coverage of 10x and an average coverage of 65x (**Table S2, S3**). These selected
223 sites were included in the analysis even if they did not appear consistently across both samples.

224 Besides the two deeply sequenced *D. magna* samples (Dap_S1 and Dap_S2), an additional 15 *D.*
225 *magna* samples denoted Dap_D1 to Dap_D16 (Dap_D7 excluded due to low quality) were bisulfite
226 sequenced across different age groups: young (9 days), mature (22 to 27 days), and old (51 to 58 days).
227 Similar approaches of alignment, methylation calling, and filtration were applied to the 15 samples. This
228 approach yielded an average of 10.9 million cytosine sites per sample, each with a minimum coverage of
229 10x, for our downstream analysis (**Table S2, S3**).

230

231 **Mitochondrial genome methylation as a negative control for non-conversion artifacts**

232 Bisulfite treatment converts unmethylated cytosines to uracils, while leaving the methylated
233 cytosines unchanged, allowing methylation to be accurately detected through sequencing. However,
234 bisulfite conversion is not 100% effective, and a small fraction (typically around 1%) of unmethylated
235 cytosines fail to deaminate and are mistakenly identified as methylated (30).

236 To distinguish between methylcytosines and unconverted cytosines we considered several criteria.
237 If cytosine dinucleotides are methylated, we expect the methylation patterns at individual sites to be
238 consistent across samples. To investigate this, we conducted correlation analyses between the Dap_S1 and
239 Dap_S2 samples across different cytosine contexts. We observed a high correlation (r = 0.949) for CpG
240 sites between the two samples, indicating reproducible methylation patterns. We also expect that
241 methylated CpG dinucleotides are present on both strands, which is often referred to as symmetric
242 methylation. In Dap_S1, we identified 1,100,329 pairs of CpG sites with non-zero methylation on both
243 strands, of which 1,040,273 pairs (94.5%) had a difference in methylation of less than 0.05. Similarly, in
244 Dap_S2, 1,204,966 CpG pairs had non-zero methylation, with 1,129,724 pairs (93.8%) showing a
245 difference below 0.05. This high degree of symmetry between strands further supports the reliability of
246 CpG methylation signals (31). By contrast, non-CpG contexts exhibited much lower correlations, with
247 CpA at r = 0.338, CpC at r = 0.222, and CpT at r = 0.249. The low correlation levels for non-CpG sites
248 suggest that these are likely artifacts of incomplete bisulfite conversion rather than true methylation.

249 Moreover, to differentiate between bisulfite non-conversion and true cytosine methylation, we
250 used the mitochondrial genome as a negative control, as previous studies have shown that mitochondrial
251 DNA is generally unmethylated (32) and have utilized this approach to assess true methylation level (33).
252 Cytosine dinucleotides in the mitochondrial genome exhibited median coverage levels exceeding 100x
253 (**Figure S2**), and this high coverage allows us to use the mitochondrial genome as a negative control.
254 Dap_S1 and Dap_S2 displayed consistent methylation patterns across all cytosine contexts (**Figure S3**)
255 with median methylation levels ranging from 0.2% to 0.5%. Non-CpG sites had third-quartile methylation
256 levels between 1.0% and 1.2%, while CpG sites exhibited a slightly higher third quartile of 1.6%. To
257 estimate the non-conversion rate in the nuclear genome, we compared the methylation levels of individual
258 nuclear cytosine sites with those in the mitochondrial genome. The average methylation levels in the
259 mitochondrial genome were comparable to or even higher than those observed in the nuclear genome
260 (**Figure S4**). Moreover, non-CpG sites in the mitochondrial genome showed a higher percentage of
261 methylation levels exceeding 20% compared to nuclear sites. However, the presence of nuclear
262 mitochondrial sequences (nuMT) (34) in *D. magna*—mitochondrial DNA fragments inserted into the

263 nuclear genome—may explain some of these effects (35). These nuMT sequences are fragments of
264 mitochondrial DNA and thus contribute ambiguity to interpreting the data and potentially skewing nuclear
265 methylation measurements by retaining mitochondrial methylation patterns or contributing additional
266 unmethylated cytosines, depending on their conversion rates. To estimate the proportion of nuMTs, we re-
267 mapped reads originally aligned to the mitochondrial genome onto the nuclear genome. We found that
268 26.1% of mitochondrial-aligned reads in Dap_S1 and 22.7% in Dap_S2 mapped to the nuclear genome
269 with a normalized Alignment Score greater than 90%. This score was calculated by dividing the
270 alignment score from BSBolt Align by the read length. This substantial fraction suggests that a portion of
271 what appears to be mitochondrial methylation may instead originate from nuMTs.
272 In contrast to non-CpG sites, CpG sites in the nuclear genome displayed higher methylation levels
273 than those in the mitochondrial genome, suggesting that CpG sites in the nuclear genome are methylated
274 rather than artifacts of non-conversion.
275
276 ***D. magna* DNA CpG sites are methylated at low levels**
277 To elucidate methylation at a global level, we computed the average methylation levels of the 97
278 contigs. CpT and CpC sites exhibited an average methylation level of approximately 1.25%, while CpA
279 methylation was slightly lower with 1.1% methylation (**Figure S5**). By contrast, CpG sites displayed
280 higher average methylation levels, around 2.05% across contigs, whose distribution of methylation was
281 significantly different from that of the non-CpG sites (p-value < 0.0001 in Wilcox test).
282 We further assessed the methylation levels at individual CpN sites and categorized corresponding
283 fractions of methylation levels (**Figure 2**). We found that the two samples had comparable methylation
284 levels, and the methylation levels of CpA, CpT, and CpC sites were distributed similarly. Around 40% of
285 the non-CpG sites had a non-zero methylation level below 0.05, while around 55% had no methylation.
286 Approximately 5% of the non-CpG sites had a methylation level above 0.05 and less than 0.2% above
287 0.20. By contrast, CpG sites are significantly hypermethylated compared to the three non-CpG cytosine
288 contexts in both samples (p-value < 0.0001 in the Wilcox test). Approximately 6% of the CpG sites had a
289 methylation level above 0.05 and around 1% of the sites above 0.20. Specifically, 0.5% of the CpG sites
290 have a methylation level above 0.80. This higher methylation frequency in CpG sites could be attributed
291 to the specificity of DNMTs, which primarily target CpG dinucleotides over non-CpG sites (36). This
292 pattern emphasizes the established role of CpG methylation in invertebrate transcriptional regulation (37),
293 further distinguishing it from non-CpG methylation contexts.

294 In addition to examining the overall methylation trends, we analyzed the methylation profiles
295 within specific groups of sequences, including DNA transposons, retrotransposons, LTR retrotransposons,
296 and non-LTR elements. While some short interspersed nuclear elements (e.g., SINE_U, SINE_B2,
297 SINE_Alu) showed localized methylation upstream or downstream of the sequences, most repetitive
298 elements exhibited constant low methylation levels.
299
300 ***D. magna* DNA CpG sites are hypomethylated upstream of TSS**
301 We next examined methylation patterns around genes, focusing on the range of 3 kilobases
302 upstream of the transcription start site (TSS) to 3 kilobases downstream of the transcription end site
303 (TES). Both samples, Dap_S1 and Dap_S2, showed consistent trends, highlighting the reproducibility of
304 these patterns. Non-CpG sites maintained a uniform methylation level of approximately 1.5% across the
305 gene and proximal regions (**Figure 3A, Figure 3B, Figure 3D**), suggesting non-CpG methylation is
306 mainly an artifact and represents background noise. In contrast, CpG methylation displayed greater
307 variability at different positions along genes. Specifically, CpG methylation levels were lowest a few
308 hundred bases upstream of the TSS (1.5% methylated) and sharply increased downstream of the TSS,
309 peaking at nearly 4.5% (**Figure 3C**). Subsequently, within the gene, CpG methylation levels gradually
310 decreased, reaching 1.5%, underscoring the enrichment on the 5' end of the genes.
311 To minimize positional artifacts from normalizing genes to a uniform distance and to provide
312 more insight into dynamic CpG methylation within genes, we grouped genes into deciles based on their
313 mean methylation levels (e.g., top 10%, 10-20%) and calculated methylation levels centered at the TSS
314 and TES. Dap_S1 (**Figure 4**) and Dap_S2 (**Figure S6**) displayed high methylation in the top 20% of
315 genes (**Figure S7**) and minimal methylation in the lower 50% of genes (**Figure S8**). Around the TSS, the
316 top 20% of genes showed markedly higher methylation levels than the rest, with methylation at the 5' end
317 exceeding 30% in the top 10% and nearly reaching 20% in the 10-20% group. At the same time,
318 methylation in the top 10% of genes peaked at 10% upstream of the TES.
319 We explored the functions of the highly methylated genes and unmethylated genes using pathway
320 enrichment analysis. Human homologs of *D. magna* genes within the top 10% methylation category
321 across both samples were significantly enriched for fundamental cellular processes in the Gene Ontology
322 Biology Process (GOBP) database, including ribonucleoprotein complex biogenesis, cytoplasmic
323 translation, mitochondrial gene expression, respiratory electron transport chain, methylation, and DNA
324 replication. Unmethylated genes showed no enrichment for any specific pathway.
325

326 ***D. magna* Exon CpG sites are more methylated than neighboring intron regions**

327 To further explore the landscape of genomic methylation, we analyzed differential methylation
328 patterns between exons and introns. Our findings reveal that exons contain a higher density of methylated
329 CpG sites (**Figure S9**). On average, exons showed a methylation rate of approximately 0.17%, whereas
330 nearby intronic regions were significantly less methylated, averaging 0.07% ($p < 0.001$ in the Wilcox
331 test). Among the exons with a mean methylation rate greater than zero, the average methylation rate is
332 8.7%, significantly higher than the 4.9% observed in methylated introns ($p < 0.001$ in Wilcoxon test).

333 We also analyzed methylation levels across exons in genes with at least five exons to understand
334 how exon position affects methylation. We observed that methylation varied significantly with exon
335 positions (**Figure 5A**). Specifically, Exon 1 shows a gradual increase in CpG methylation, peaking near
336 its 3' end, followed by a sharp drop at the transition to the adjacent intron. This pattern of exon
337 hypermethylation and intron hypomethylation is primarily driven by the top 10% of methylated genes
338 (**Figure 5B**). Methylation levels continued to rise in Exon 2, reaching a peak of nearly 8% in Exon 3
339 before decreasing (**Figure 5A**).

340

341 ***D. magna*'s global and local CpG methylation patterns are weakly associated with age**

342 To determine how the methylation pattern changes with age, we first conducted a global analysis
343 of CpG methylation levels across three age groups: young, mature, and old. The average methylation
344 levels were 3.426% in the young group, 3.386% in the mature group, and 3.311% in the old group,
345 showing a slight decrease with age; however, none of these differences reached statistical significance
346 (**Figure 6A**). We also aggregated methylation values for CpG sites present in at least 80% of samples,
347 imputed missing values, and constructed a CpG matrix. Visualization of this matrix using UMAP did not
348 reveal clear clustering by age group, indicating a general absence of global age-related methylation
349 patterns (**Figure 6B**). We further filtered the CpG matrix to retain CpG sites in genes with at least 10%
350 methylation (562 genes in total) in at least 80% of the 17 samples. However, UMAP visualization of the
351 filtered matrix of the filtered matrix also showed no age-related methylation patterns (**Figure S10**).
352 Furthermore, to identify specific CpG sites that could serve as indicators of age, we trained an epigenetic
353 clock through Lasso Leave-One-Out cross-validation regression (**Figure S11**). However, the correlation
354 between predicted and actual ages was not significant, indicating that age-associated changes in the
355 methylation of CpG sites were not robust enough to build an accurate epigenetic clock.

356 Next, we explored age-related changes in CpG methylation at the gene level. While meta-gene
357 methylation analysis demonstrated a consistent pattern across age groups (**Figure 6C**), closer examination

358 of the differences between age groups revealed a weak trend of decreasing methylation with advancing
359 age (**Figure S12**). However, random permutation tests at each position showed no statistically significant
360 differences across all sites for the three pairwise age group comparisons. We also performed differentially
361 methylated regions (DMR) analysis and linear regression analyses at the individual gene level, using the
362 mean CpG methylation level as the dependent variable and age as the predictor. Neither any regions nor
363 genes showed significant associations with age, indicating a lack of robust gene-level methylation
364 changes.
365

366 **DISCUSSION**

367 In this study, our primary focus was elucidating the genome-wide and gene-level methylation
368 patterns in *Daphnia magna* and analyzing the age-associated variations in methylation levels. One key
369 area of interest was the DNA methyltransferases in *D. magna*. Maintenance methyltransferase
370 *Dma*DNMT1 and *de novo* methyltransferase *Dma*DNMT3.2 were both functional but expressed at low
371 levels. In contrast, the non-functional DNMT3.1 exhibited higher expression levels and a potential
372 association with aging, suggesting functions beyond DNA methylation. For example, DNMT3.1 has been
373 shown to regulate growth and reproduction under starvation conditions (10).

374 To explore the evolutionary relationships of invertebrate DNA methyltransferases, we compared
375 *Dma*DNMTs with DNMTs from other invertebrates. Within the phylum Arthropoda, species in the
376 subphylum Crustacea, including *Daphnia pulex*, *Procambarus virginalis* (marbled crayfish), *Parhyale*
377 *hawaiensis*, *Penaeus vannamei*, and *Hyalella azteca*, retain at least one DNMT3. In contrast, several
378 crustaceans, such as *Armadillidium vulgare*, *Calanus finmarchicus*, *Eurytemora affinis*, *Lepeophtheirus*
379 *salmonis*, and *Tigriopus californicus*, have lost DNMT3 (38,39). Expanding to the Hexapoda subphylum,
380 which shares a common arthropod ancestor with crustaceans, DNMT3 is largely conserved in bees and
381 ants, with *Solenopsis invicta* (red imported fire ant) and *Apis mellifera* (honey bee) possessing one
382 DNMT3 (39–41). However, DNMT3 appears to be absent in most wasps, flies, butterflies, and moths,
383 including *Polistes dominula*, *Drosophila melanogaster*, *Bombyx mori* (silkworm moth), and *Danaus*
384 *plexippus* (monarch butterfly) (39,42,43). Moving further from Arthropoda, DNMT3 is also present in
385 other invertebrate phyla. In Mollusca, *Crassostrea gigas* (oyster) retains functional DNMT3 (44).
386 Similarly, in Annelida, *Capitella teleta* and *Ophryotrocha fusiformis* possess DNMT3, whereas
387 *Dinophilus gyrociliatus* lacks it (45). The observed diversity in the presence and functionality of DNMT3
388 among invertebrates reflects adaptive modifications to their unique genomic and environmental demands,
389 with *D. magna* representing one variation of this evolutionary landscape.

390 Most invertebrates possess a maintenance methyltransferase DNMT1 with a functional MTase
391 protein domain. However, certain species, including *D. melanogaster*, *Aedes aegypti*, *Anopheles gambiae*,
392 and *Caenorhabditis elegans* lack DNMT1 altogether (11,38–45). As observed in *D. magna*, the N-
393 terminal DMAP-1 binding domain has been lost in many invertebrates, including arthropods (*A.*
394 *mellifera*), annelids (*C. teleta* and *O. fusiformis*), ctenophores *(Pleurobrachia bachei*), brachiopods
395 (*Lingula anatina*) (45–47). This supports previous findings that the DMAP-1 binding domain is
396 conserved in chordates but largely absent in invertebrates (48).

397 We cultured 17 *D. magna* samples of different ages and conducted whole-genome bisulfite
398 sequencing, achieving a high-coverage methylome with an approximate coverage of 60x. This allows us
399 to analyze the methylation patterns across genome, gene, and exon levels. Globally, *D. magna* exhibited
400 an average CpG methylation level of 2%. In comparison, mammals such as mice have an average CpG
401 methylation level of around 80% (49). One possible explanation for this low methylation level is the
402 reduced expression of *Dma*DNMT1 and the absence of the DMAP-1 binding domain. The DMAP-1
403 binding domain facilitates DNMT1's interaction with DMAP-1, a co-repressor that aids its methylation
404 maintenance activity (50). However, the correlation between the absence of DMAP-1 binding domain and
405 reduced methylation appears weak and does not hold consistently across invertebrates. For example, the
406 annelids *C. teleta* and *O. fusiformis* also lack no DMAP-1 binding domain, yet more than 17% of their
407 CpG sites remain methylated (45). Similarly, *A. mellifera* lacks this domain but maintains global CpG
408 methylation levels above 40% (51). These discrepancies suggest the factors contributing to *D. magna*'s
409 low methylation levels remain unknown.
410 *D. magna* has an average gene body methylation of around 3%, slightly higher than the global
411 methylation level. Gene body methylation refers to the addition of methyl groups, typically at CpG sites,
412 within the coding regions of genes. It is often associated with actively transcribed genes, where it may
413 help regulate splicing, reduce spurious transcription, and maintain genome stability (52). Gene body
414 methylation is widely observed in animals, plants, and some fungi (33). The mosaic DNA methylation
415 with a high level in gene bodies and lower level in intergenic regions was observed in many other
416 invertebrates, including sea urchin, lancelet, honey bee *A. mellifera*, green peach aphid *Myzus persicae*,
417 and *O. fusiformis and C. teleta* (45,53–55). However, *D. magna*'s gene body methylation is lower than
418 the other invertebrates, which may be attributed to the absence of a functional PWWP domain in
419 DNMT3.2. Since the PWWP domain binds to H3K36me2 and H3K36me3, markers typically found in
420 transcribed regions, its absence could lead to a reduced recognition of H3K36-methylated gene bodies by
421 the active DNMT3.2, resulting in low methylation levels (56–58). Supporting this, H3K36me3
422 enrichment in gene bodies has been observed in other invertebrates, including *Nematostella vectensis*,
423 *Ciona intestinalis*, *A. mellifera*, and *Bombyx mori* (59).
424 In examining the methylation patterns across gene bodies and surrounding regions, we observed
425 that the genes are hypomethylated upstream of the TSS and hypermethylated downstream of the TSS,
426 with methylation levels decreasing along the genes. This pattern aligns with findings in the annelids *O.*
427 *fusiformis* and *C. teleta*, where a similar trend of hypomethylation at TSS has been reported (45). The
428 hypomethylation at the TSS likely results from a mechanism similar to that described in mammals, where

429 the ADD domain of active DNMT3 selectively binds to unmethylated H3K4 regions (60). As mammalian
430 promoters are typically rich in methylated H3K4, this prevents DNMT3 from binding and consequently
431 blocks DNA methylation in mammalian systems (61). A comparable mechanism may operate in *Daphnia*
432 *magna*, as previous research has shown a high enrichment of H3K4me3 upstream of the actively
433 transcribed *Actin* gene (9). Furthermore, a strong correlation between gene expression and H3K4me3
434 levels at promoter regions in *Daphnia pulex* further supports this regulatory mechanism in *D. magna* (62).
435 We observed significantly higher methylation levels in exons compared to introns, which was also
436 reported in *O. fusiformis*, *C. gigas*, and *A. mellifera* (44,45,49). This differential methylation is likely
437 influenced by nucleosome positioning, as DNA methyltransferases preferentially target nucleosome-
438 bound DNA (63). Consequently, the enrichment of nucleosomes on exons leads to higher methylation in
439 these regions, suggesting a role for DNA methylation in exon definition and alternative splicing
440 regulation (64,65).
441 Our analysis of *Daphnia magna* samples revealed minor, insignificant decreases in global and
442 gene-specific methylation levels with age as well as no significant age-related clustering. This contrasts
443 with vertebrates, where DNA methylation patterns are highly dynamic and exhibit notable changes during
444 aging (66). Thus, the relatively constant DNA methylation level of *D. magna* across age underlines the
445 possibility DNA methylation is less coupled to developmental changes in gene expression than in
446 vertebrates, possibly due to the different structure of the DNA methyltransferases. At the same time, our
447 attempt to build an epigenetic clock failed for *D. magna*. This failure is likely due to the low overall CpG
448 methylation levels compared to mammals and the small magnitude of methylation changes with age,
449 making it difficult to identify age-associated patterns necessary for clock construction. Indeed, only a few
450 epigenetics clocks have been reported for invertebrates. Recently, an epigenetic clock on *Nasonia*
451 *vitripennis*, the jewel wasp, using 19 age-predictive CpG sites was found to have a Spearman's P of 0.94
452 for the correlation between predicted and actual age (67). However, the fact that the clock CpG sites were
453 pre-selected for their age association indicates possible overfitting to their samples. Thus, we still lack
454 robust evidence that epigenetic clocks can be generated for invertebrates.
455 Although no epigenetic clocks were established, we observed a slight decline in CpG site
456 methylation levels with aging in *D. magna*. This pattern of epigenetic erosion is pronounced in
457 invertebrates during development (68,69). For example, in *A. mellifera* (honey bee), exon methylation
458 decreases from sperm and embryo to drone and worker larvae (70). Similarly, annelids such as *O.*
459 *fusiformis* and *C. teleta* experience global methylation loss from embryonic to adult ages (45), while
460 deuterostomes like sea urchin and lancelet display lower methylation levels in adulthood compared to

earlier developmental stages (53). This feature of global hypomethylation has been reported as a consequence of heterochromatin loss, a hallmark of aging across diverse eukaryotes (71).

In this study, our primary emphasis was on the *D. magna* Xinb3 clone. The methylation profiles we elucidated may be slightly altered in other *D. magna* strains. Future research should explore the methylation patterns in additional clones to achieve a more comprehensive understanding. Given the limited correlation between DNA methylation and chronological age, our future attention will shift towards the influence of environmental factors, including temperature and water composition, on methylation dynamics.

Declarations

LP was supported by the quadraScope Ventures fund and McKenzie Family Charitable Trust.

Disclosure of interest

The authors declare that the research was conducted in the absence of any commercial or financial relationships that could be construed as potential conflicts of interest.

Data availability of the Statement

Bisulfite sequencing data and CGmatrix generated in this study have been deposited within the Gene Expression Omnibus (GEO) repository, accession number GSE267859.

481 **Reference**

482 1. Ebert D. Ecology, epidemiology, and evolution of parasitism in Daphnia. National Library of
483 Medicine; 2005.
484 2. Tkaczyk A, Bownik A, Dudka J, Kowal K, Ślaska B. Daphnia magna model in the toxicity
485 assessment of pharmaceuticals: A review. Sci Total Environ. 2021;763:143038.
486 3. Vandegehuchte MB, Lemière F, Vanhaecke L, Berghe WV, Janssen CR. Direct and transgenerational
487 impact on Daphnia magna of chemicals with a known effect on DNA methylation. Comp Biochem
488 Physiol Part C Toxicol Pharmacol. 2010;151(3):278–85.
489 4. Watson RE, McKim JM, Cockerell GL, Goodman JI. The value of DNA methylation analysis in
490 basic, initial toxicity assessments. Toxicol Sci. 2004;79(1):178–88.
491 5. Bonini NM, Berger SL. The sustained impact of model organisms—in genetics and epigenetics.
492 Genetics. 2017;205(1):1–4.
493 6. Hearn J, Plenderleith F, Little TJ. DNA methylation differs extensively between strains of the same
494 geographical origin and changes with age in Daphnia magna. Epigenetics Chromatin. 2021;14:1–14.
495 7. Smith ZD, Meissner A. DNA methylation: roles in mammalian development. Nat Rev Genet.
496 2013;14(3):204–20.
497 8. Kvist J, Gonçalves Athanàsio C, Shams Solari O, Brown JB, Colbourne JK, Pfrender ME, et al.
498 Pattern of DNA methylation in Daphnia: evolutionary perspective. Genome Biol Evol.
499 2018;10(8):1988–2007.
500 9. Lindeman LC, Thaulow J, Song Y, Kamstra JH, Xie L, Asselman J, et al. Epigenetic, transcriptional
501 and phenotypic responses in two generations of Daphnia magna exposed to the DNA methylation
502 inhibitor 5-azacytidine. Environ Epigenetics. 2019;5(3):dvz016.
503 10. Nguyen ND, Matsuura T, Kato Y, Watanabe H. DNMT3. 1 controls trade-offs between growth,
504 reproduction, and life span under starved conditions in Daphnia magna. Sci Rep. 2021;11(1):7326.
505 11. Lyko F. The DNA methyltransferase family: a versatile toolkit for epigenetic regulation. Nat Rev
506 Genet. 2018;19(2):81–92.
507 12. Duan R, Fu Q, Sun Y, Li Q. Epigenetic clock: A promising biomarker and practical tool in aging.
508 Ageing Res Rev. 2022;81:101743.
509 13. Horvath S. DNA methylation age of human tissues and cell types. Genome Biol. 2013;14:1–20.
510 14. Horvath S, Raj K. DNA methylation-based biomarkers and the epigenetic clock theory of ageing. Nat
511 Rev Genet. 2018;19(6):371–84.
512 15. Klüttgen B, Dülmer U, Engels M, Ratte H. ADaM, an artificial freshwater for the culture of

513 zooplankton. Water Res. 1994;28(3):743–6.
514 16. Cho Y, Jonas-Closs RA, Yampolsky LY, Kirschner MW, Peshkin L. Intelligent high-throughput
515 intervention testing platform in Daphnia. Aging Cell. 2022;21(3):e13571.
516 17. Fields PD, Obbard DJ, McTaggart SJ, Galimov Y, Little TJ, Ebert D. Mitogenome phylogeographic
517 analysis of a planktonic crustacean. Mol Phylogenet Evol. 2018;129:138–48.
518 18. Farrell C, Thompson M, Tosevska A, Oyetunde A, Pellegrini M. BiSulfite Bolt: A bisulfite
519 sequencing analysis platform. Gigascience. 2021;10(5):giab033.
520 19. Danecek P, Bonfield JK, Liddle J, Marshall J, Ohan V, Pollard MO, et al. Twelve years of SAMtools
521 and BCFtools. Gigascience. 2021;10(2):giab008.
522 20. Guo W, Zhu P, Pellegrini M, Zhang MQ, Wang X, Ni Z. CGmapTools improves the precision of
523 heterozygous SNV calls and supports allele-specific methylation detection and visualization in
524 bisulfite-sequencing data. Bioinformatics. 2018;34(3):381–7.
525 21. Yu G, Wang LG, Han Y, He QY. clusterProfiler: an R package for comparing biological themes
526 among gene clusters. Omics J Integr Biol. 2012;16(5):284–7.
527 22. Thorvaldsdóttir H, Robinson JT, Mesirov JP. Integrative Genomics Viewer (IGV): high-performance
528 genomics data visualization and exploration. Brief Bioinform. 2013;14(2):178–92.
529 23. McInnes L, Healy J, Melville J. Umap: Uniform manifold approximation and projection for
530 dimension reduction. ArXiv Prepr ArXiv180203426. 2018;
531 24. Pedregosa F, Varoquaux G, Gramfort A, Michel V, Thirion B, Grisel O, et al. Scikit-learn: Machine
532 learning in Python. J Mach Learn Res. 2011;12:2825–30.
533 25. Jühling F, Kretzmer H, Bernhart SH, Otto C, Stadler PF, Hoffmann S. Metilene: fast and sensitive
534 calling of differentially methylated regions from bisulfite sequencing data. Genome Res.
535 2016;26(2):256–62.
536 26. Dua I, Pearson AC, Lowman RL, Peshkin L, Yampolsky LY. Post-senescence reproductive rebound
537 in Daphnia associated with reversal of age-related transcriptional changes. GeroScience. 2024;1–20.
538 27. Love MI, Huber W, Anders S. Moderated estimation of fold change and dispersion for RNA-seq data
539 with DESeq2. Genome Biol. 2014;15:1–21.
540 28. Jones P, Binns D, Chang HY, Fraser M, Li W, McAnulla C, et al. InterProScan 5: genome-scale
541 protein function classification. Bioinformatics. 2014;30(9):1236–40.
542 29. Nguyen Ba AN, Pogoutse A, Provart N, Moses AM. NLStradamus: a simple Hidden Markov Model
543 for nuclear localization signal prediction. BMC Bioinformatics. 2009;10:1–11.
544 30. Genereux DP, Johnson WC, Burden AF, Stöger R, Laird CD. Errors in the bisulfite conversion of

545 DNA: modulating inappropriate-and failed-conversion frequencies. Nucleic Acids Res.
546 2008;36(22):e150–e150.
547 31. Bird AP. Use of restriction enzymes to study eukaryotic DNA methylation: II. The symmetry of
548 methylated sites supports semi-conservative copying of the methylation pattern. J Mol Biol.
549 1978;118(1):49–60.
550 32. Mechta M, Ingerslev LR, Fabre O, Picard M, Barrès R. Evidence suggesting absence of mitochondrial
551 DNA methylation. Front Genet. 2017;8:166.
552 33. Zemach A, McDaniel IE, Silva P, Zilberman D. Genome-wide evolutionary analysis of eukaryotic
553 DNA methylation. Science. 2010;328(5980):916–9.
554 34. Bensasson D, Zhang DX, Hartl DL, Hewitt GM. Mitochondrial pseudogenes: evolution's misplaced
555 witnesses. Trends Ecol Evol. 2001;16(6):314–21.
556 35. Kowal K, Tkaczyk A, Pierzchała M, Bownik A, Ślaska B. Identification of mitochondrial dna
557 (Numts) in the nuclear genome of daphnia magna. Int J Mol Sci. 2020;21(22):8725.
558 36. Moore LD, Le T, Fan G. DNA methylation and its basic function. Neuropsychopharmacology.
559 2013;38(1):23–38.
560 37. Suzuki MM, Kerr AR, De Sousa D, Bird A. CpG methylation is targeted to transcription units in an
561 invertebrate genome. Genome Res. 2007;17(5):625–31.
562 38. Lewis SH, Ross L, Bain SA, Pahita E, Smith SA, Cordaux R, et al. Widespread conservation and
563 lineage-specific diversification of genome-wide DNA methylation patterns across arthropods. PLoS
564 Genet. 2020;16(6):e1008864.
565 39. Engelhardt J, Scheer O, Stadler PF, Prohaska SJ. Evolution of DNA methylation across ecdysozoa. J
566 Mol Evol. 2022;90(1):56–72.
567 40. Wang Y, Jorda M, Jones PL, Maleszka R, Ling X, Robertson HM, et al. Functional CpG methylation
568 system in a social insect. Science. 2006;314(5799):645–7.
569 41. Kay S, Skowronski D, Hunt BG. Developmental DNA methyltransferase expression in the fire ant
570 Solenopsis invicta. Insect Sci. 2018;25(1):57–65.
571 42. Krauss V, Reuter G. DNA methylation in Drosophila—a critical evaluation. Prog Mol Biol Transl
572 Sci. 2011;101:177–91.
573 43. Planques A, Kerner P, Ferry L, Grunau C, Gazave E, Vervoort M. DNA methylation atlas and
574 machinery in the developing and regenerating annelid Platynereis dumerilii. BMC Biol.
575 2021;19(1):148.
576 44. Wang X, Li Q, Lian J, Li L, Jin L, Cai H, et al. Genome-wide and single-base resolution DNA

577 methylomes of the Pacific oyster Crassostrea gigas provide insight into the evolution of invertebrate
578 CpG methylation. BMC Genomics. 2014;15:1–12.
579 45. Guynes K, Sarre LA, Carrillo-Baltodano AM, Davies BE, Xu L, Liang Y, et al. Annelid methylomes
580 reveal ancestral developmental and aging-associated epigenetic erosion across Bilateria. Genome
581 Biol. 2024;25(1):204.
582 46. Dabe EC, Sanford RS, Kohn AB, Bobkova Y, Moroz LL. DNA methylation in basal metazoans:
583 insights from ctenophores. Integr Comp Biol. 2015;55(6):1096–110.
584 47. Gerdol M, La Vecchia C, Strazzullo M, De Luca P, Gorbi S, Regoli F, et al. Evolutionary history of
585 DNA methylation related genes in Bivalvia: new insights from Mytilus galloprovincialis. Front Ecol
586 Evol. 2021;9:698561.
587 48. Albalat R. Evolution of DNA-methylation machinery: DNA methyltransferases and methyl-DNA
588 binding proteins in the amphioxus Branchiostoma floridae. Dev Genes Evol. 2008;218:691–701.
589 49. Feng S, Cokus SJ, Zhang X, Chen PY, Bostick M, Goll MG, et al. Conservation and divergence of
590 methylation patterning in plants and animals. Proc Natl Acad Sci. 2010;107(19):8689–94.
591 50. Lee GE, Kim JH, Taylor M, Muller MT. DNA methyltransferase 1-associated protein (DMAP1) is a
592 co-repressor that stimulates DNA methylation globally and locally at sites of double strand break
593 repair. J Biol Chem. 2010;285(48):37630–40.
594 51. Wang H, Liu Z, Wang Y, Ma L, Zhang W, Xu B. Genome-wide differential DNA methylation in
595 reproductive, morphological, and visual system differences between queen bee and worker bee (Apis
596 mellifera). Front Genet. 2020;11:770.
597 52. Jones PA. Functions of DNA methylation: islands, start sites, gene bodies and beyond. Nat Rev
598 Genet. 2012;13(7):484–92.
599 53. Skvortsova K, Bertrand S, Voronov D, Duckett PE, Ross SE, Magri MS, et al. Active DNA
600 demethylation of developmental cis-regulatory regions predates vertebrate origins. Sci Adv.
601 2022;8(48):eabn2258.
602 54. Suzuki MM, Bird A. DNA methylation landscapes: provocative insights from epigenomics. Nat Rev
603 Genet. 2008;9(6):465–76.
604 55. Klughammer J, Romanovskaia D, Nemc A, Posautz A, Seid CA, Schuster LC, et al. Comparative
605 analysis of genome-scale, base-resolution DNA methylation profiles across 580 animal species. Nat
606 Commun. 2023;14(1):232.
607 56. Dukatz M, Holzer K, Choudalakis M, Emperle M, Lungu C, Bashtrykov P, et al. H3K36me2/3
608 binding and DNA binding of the DNA methyltransferase DNMT3A PWWP domain both contribute

609 to its chromatin interaction. J Mol Biol. 2019;431(24):5063–74.
610 57. Kolasinska-Zwierz P, Down T, Latorre I, Liu T, Liu XS, Ahringer J. Differential chromatin marking
611 of introns and expressed exons by H3K36me3. Nat Genet. 2009;41(3):376–81.
612 58. Weinberg DN, Papillon-Cavanagh S, Chen H, Yue Y, Chen X, Rajagopalan KN, et al. The histone
613 mark H3K36me2 recruits DNMT3A and shapes the intergenic DNA methylation landscape. Nature.
614 2019;573(7773):281–6.
615 59. Nanty L, Carbajosa G, Heap GA, Ratnieks F, van Heel DA, Down TA, et al. Comparative
616 methylomics reveals gene-body H3K36me3 in Drosophila predicts DNA methylation and CpG
617 landscapes in other invertebrates. Genome Res. 2011;21(11):1841–50.
618 60. Otani J, Nankumo T, Arita K, Inamoto S, Ariyoshi M, Shirakawa M. Structural basis for recognition
619 of H3K4 methylation status by the DNA methyltransferase 3A ATRX–DNMT3–DNMT3L domain.
620 EMBO Rep. 2009;10(11):1235–41.
621 61. Bernstein BE, Mikkelsen TS, Xie X, Kamal M, Huebert DJ, Cuff J, et al. A bivalent chromatin
622 structure marks key developmental genes in embryonic stem cells. Cell. 2006;125(2):315–26.
623 62. Kvist J, Athanàsio CG, Pfrender ME, Brown JB, Colbourne JK, Mirbahai L. A comprehensive
624 epigenomic analysis of phenotypically distinguishable, genetically identical female and male Daphnia
625 pulex. BMC Genomics. 2020;21:1–17.
626 63. Chodavarapu RK, Feng S, Bernatavichute YV, Chen PY, Stroud H, Yu Y, et al. Relationship between
627 nucleosome positioning and DNA methylation. Nature. 2010;466(7304):388–92.
628 64. Ehrlich M, Lacey M. DNA methylation and differentiation: silencing, upregulation and modulation of
629 gene expression. Epigenomics. 2013;5(5):553–68.
630 65. Shayevitch R, Askayo D, Keydar I, Ast G. The importance of DNA methylation of exons on
631 alternative splicing. Rna. 2018;24(10):1351–62.
632 66. Meehan RR, Stancheva I. DNA methylation and control of gene expression in vertebrate
633 development. Essays Biochem. 2001;37:59–70.
634 67. Brink K, Thomas C, Jones A, Chan T, Mallon E. Exploring the ageing methylome in the model
635 insect, Nasonia vitripennis. BMC Genomics. 2024;25(1):305.
636 68. Kane AE, Sinclair DA. Epigenetic changes during aging and their reprogramming potential. Crit Rev
637 Biochem Mol Biol. 2019;54(1):61–83.
638 69. Yu G, Wu Q, Gao Y, Chen M, Yang M. The epigenetics of aging in invertebrates. Int J Mol Sci.
639 2019;20(18):4535.
640 70. Harris KD, Lloyd JP, Domb K, Zilberman D, Zemach A. DNA methylation is maintained with high

641 fidelity in the honey bee germline and exhibits global non-functional fluctuations during somatic
642 development. Epigenetics Chromatin. 2019;12:1–18.
643 71. Ciccarone F, Tagliatesta S, Caiafa P, Zampieri M. DNA methylation dynamics in aging: how far are
644 we from understanding the mechanisms? Mech Ageing Dev. 2018;174:3–17.
645

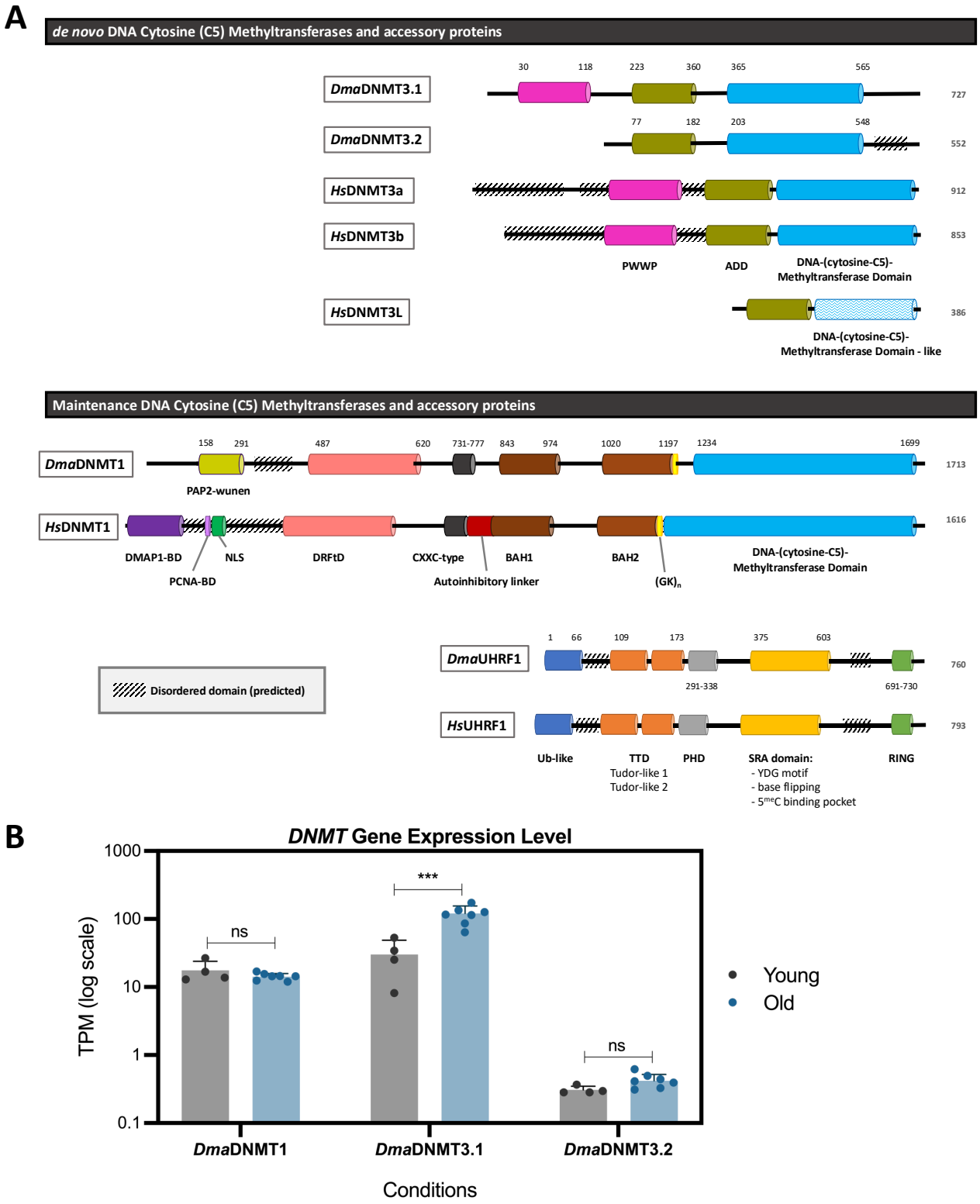

Figure 1. The comparison of DNA (C5) methyltransferases and accessory proteins of *D. magna* and *H. sapiens* and the gene expression levels under different conditions. (A) Domain structures of *de novo* and maintenance DNA methyltransferases and accessory proteins in *Daphnia magna* and *Homo sapiens* were predicted using InterProScan. Colored boxes represent the functional domains, with numbers indicating their respective positions along the protein sequence. Diagonal black-striped boxes indicate a predicted disordered consensus sequence. **(B)** Gene expression levels (TPM on log scale) of three DNMT genes (*Dma*DNMT1, *Dma*DNMT3.1, and *Dma*DNMT3.2) in young and old *D. magna* individuals. Bars represent the mean expression levels, and error bars denote standard deviation (SD). Statistical significance between conditions for each gene was assessed using a two-sided Student's t-test, with significance indicated as follows: $P < 0.001$ (***) and nonsignificant (ns). Expression levels of *Dma*DNMT1 and *Dma*DNMT3.2 showed no significant differences between the groups, while *Dma*DNMT3.1 expression was significantly different in young individuals compared to the old group.

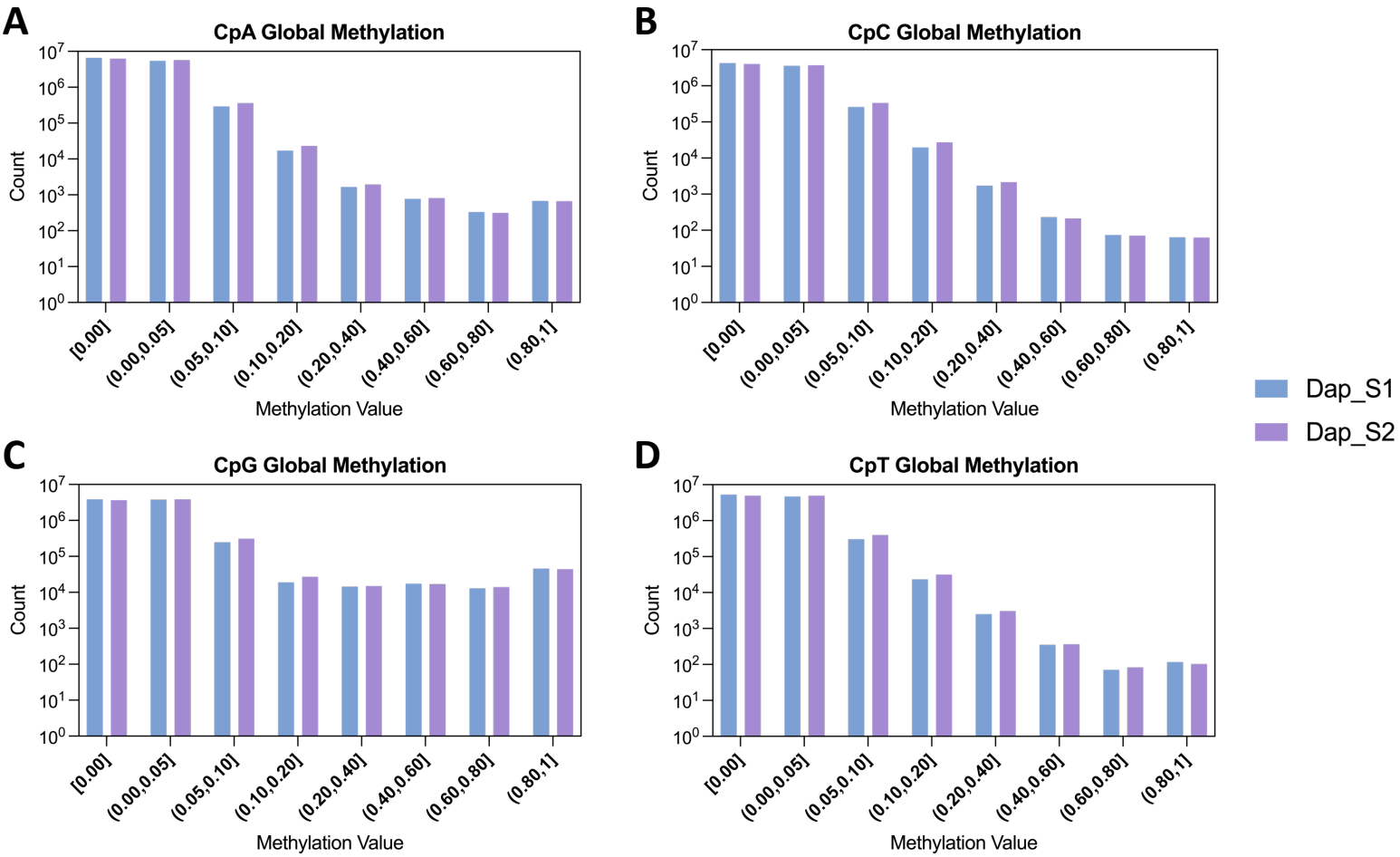

Figure 2. Global DNA methylation levels at CpN sites of two deeply sequenced samples. The count distribution of methylation levels for individual CpN sites is shown. **(A)** CpA, **(B)** CpC, and **(D)** CpT sites exhibit comparably low methylation levels. **(C)** CpG sites display a significantly higher degree of methylation overall.

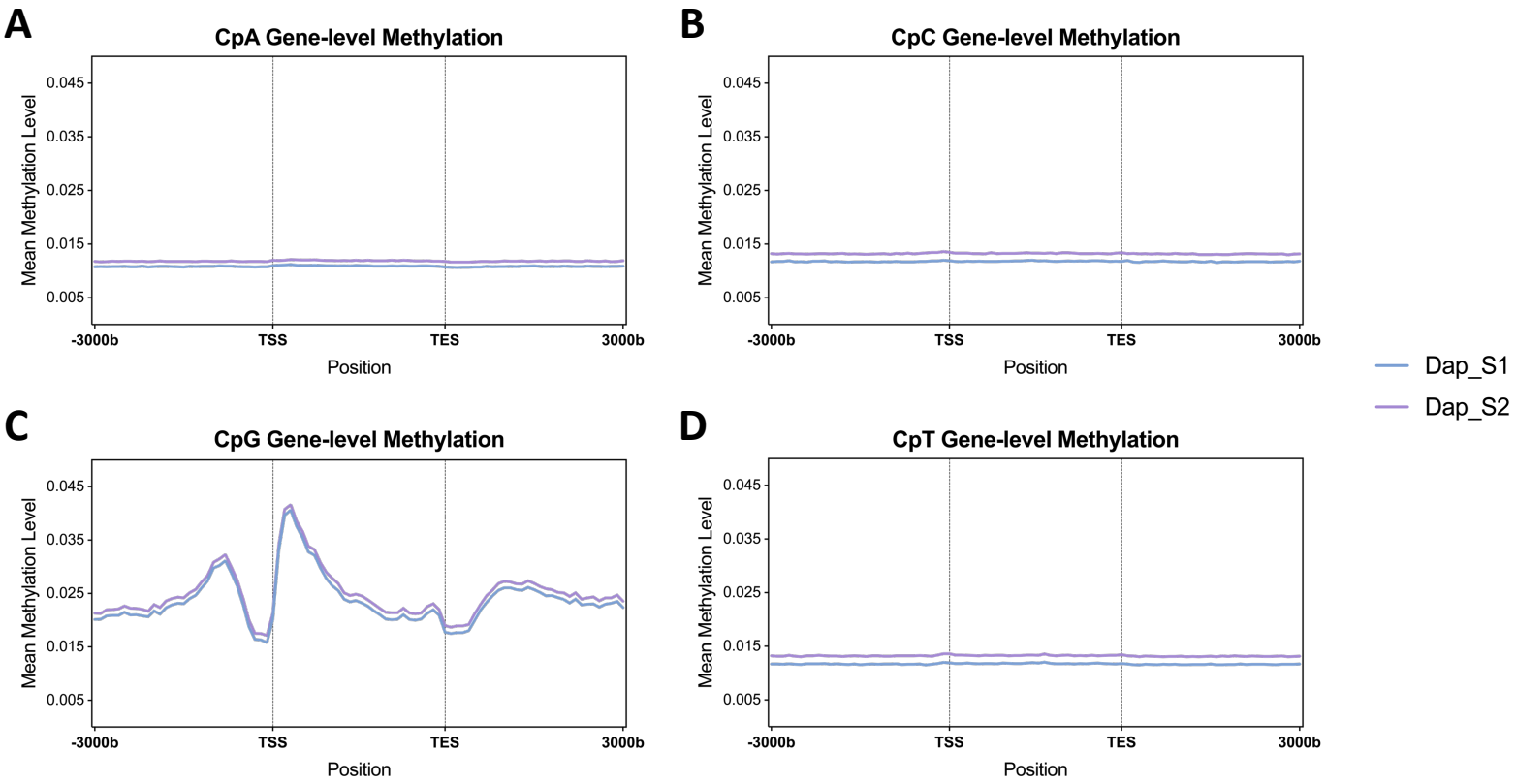

Figure 3. Gene-level DNA CpN methylation levels in two deeply sequenced samples, spanning 3 kilobases (kb) upstream transcription start sites (TSS) and 3 kb downstream of transcription end sites (TES). Each line depicts the average gene methylation value for **(A)** CpA, **(B)** CpC, **(C)** CpG, and **(D)** CpT for a sample. Non-CpG sites exhibited uniformly low methylation levels, whereas CpG sites manifest a distinctive pattern. These sites have lower methylation levels at TSS compared to regions upstream and downstream.

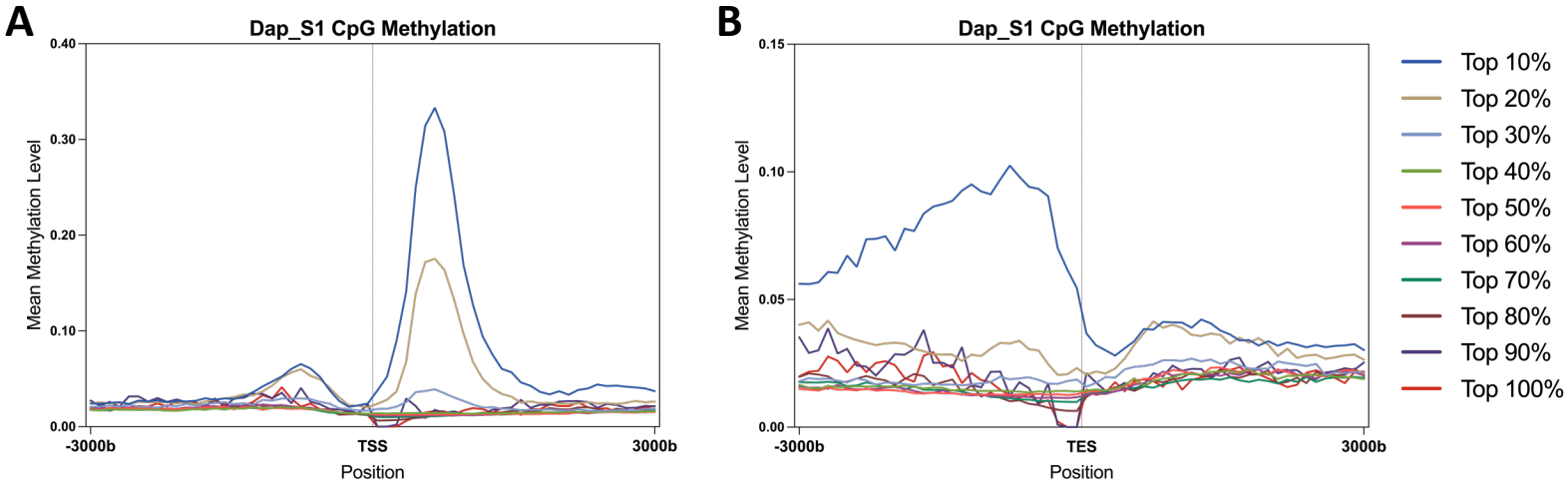

Figure 4. Gene-level CpG Methylation Patterns Centered around TSS and TES for Dap_S1, spanning 3 kilobases (kb) upstream and downstream of transcription start sites (TSS) and transcription end sites (TES). Genes were divided into 10 groups based on their mean methylation levels. Each line represents the average methylation level within each group, centered around **(A)** the transcription start site (TSS) and **(B)** the transcription end site (TES). For example, Top 20% in legend represents the top 10-20% group.

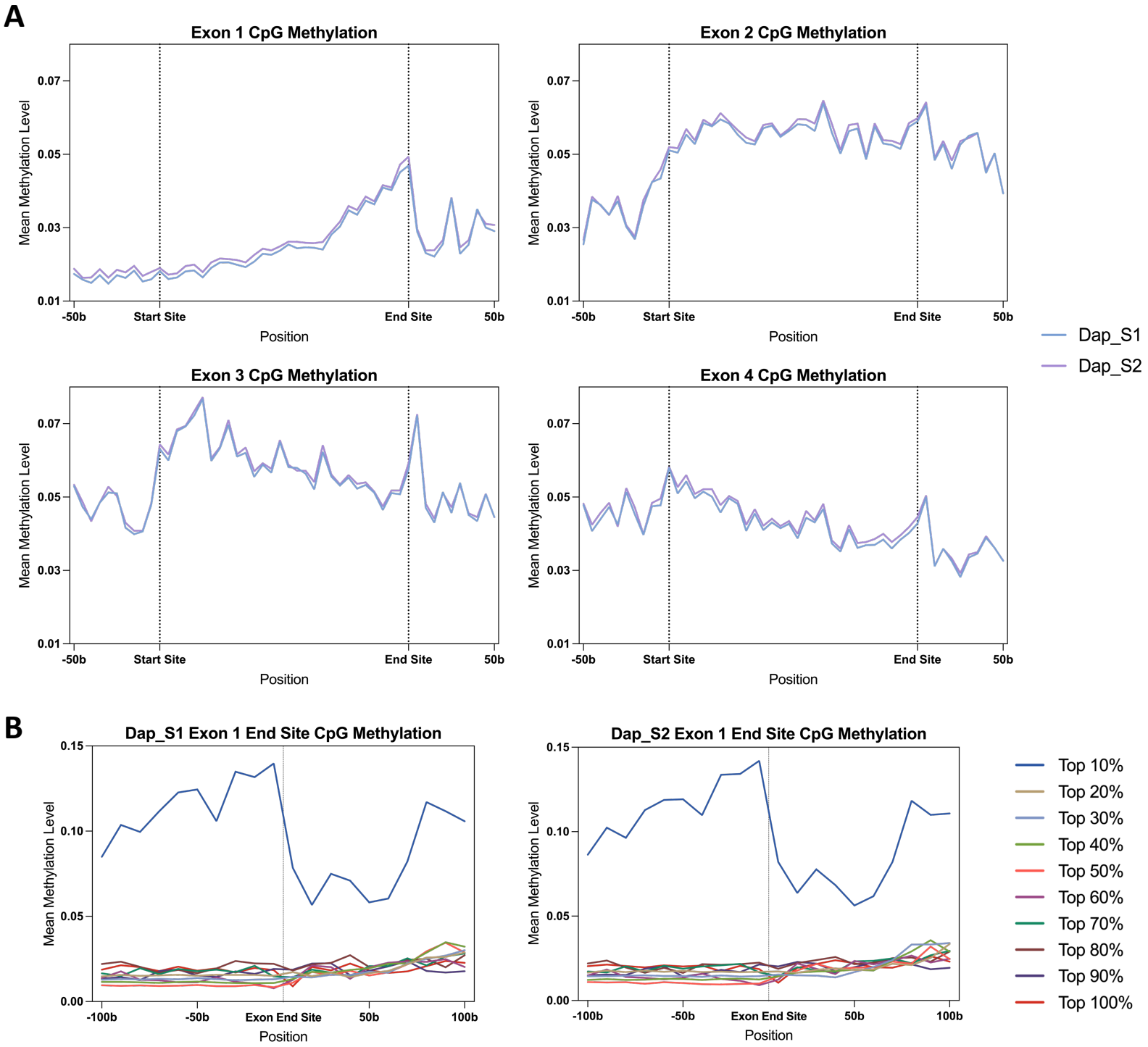

Figure 5. Exon-level CpG Methylation Patterns in two deeply sequenced samples. (A) CpG methylation levels of Exon 1 to Exon 4 from genes with more than 5 exons are demonstrated. Exon 1 shows a gradual increase in CpG methylation, peaking near its 3' end. Methylation levels continued to rise in Exon 2, reaching a peak of nearly 8% in Exon 3 before decreasing. **(B)** Genes were divided into 10 groups based on their mean methylation levels in Exon 1. Each line represents the average methylation level within each group, centered around Exon 1 end site, with 100b up- and downstream of each region. In top 10% genes, there is a sharp drop in methylation transitioning from Exon 1 to the adjacent intron.

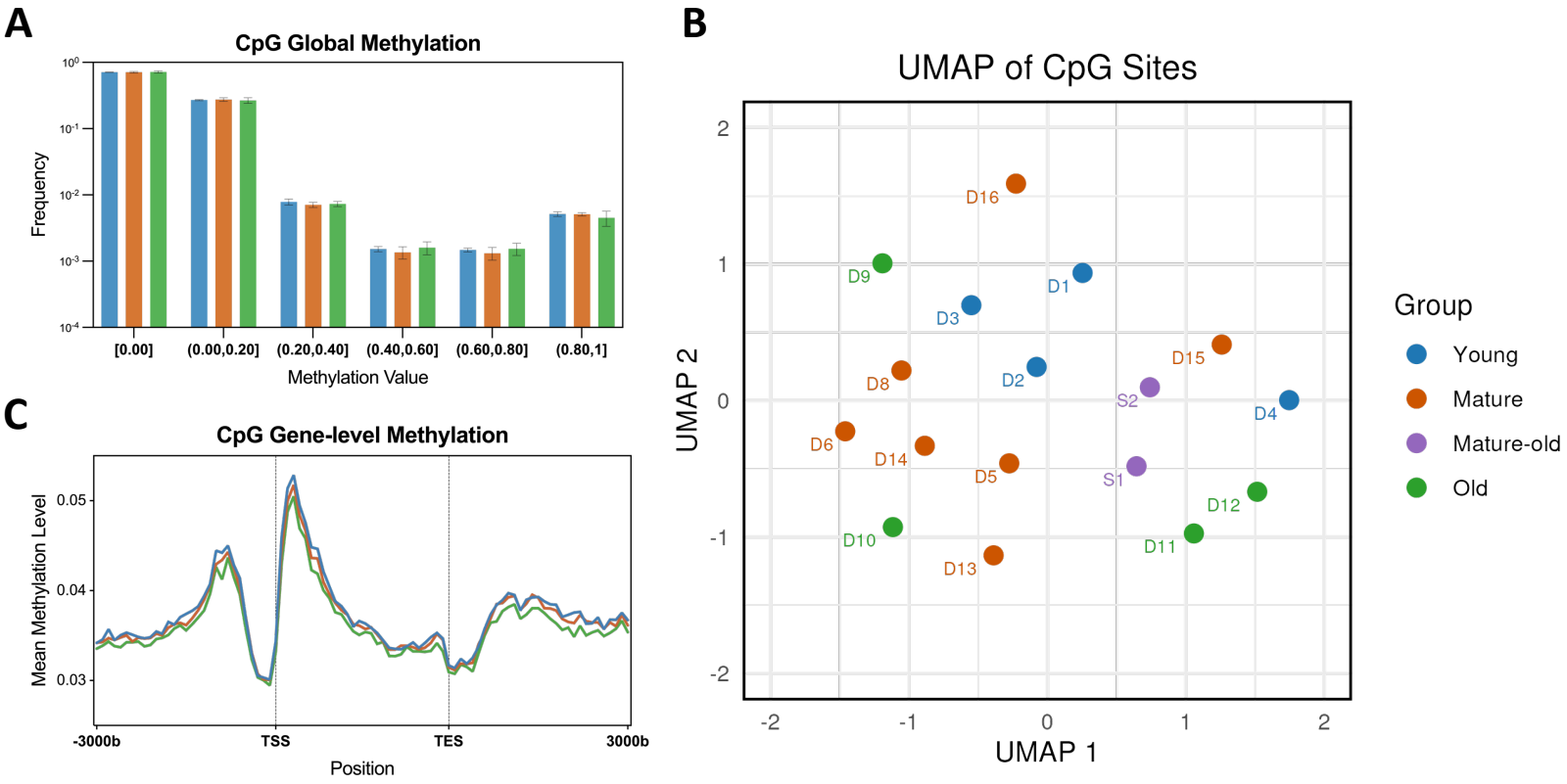

Figure 6. CpG methylation patterns across age groups demonstrate weak relation to age. (A) Methylation levels of individual CpG sites in each group are presented as the frequency distribution. **(B)** The UMAP visualization of matrix with CpG sites present in at least 80% of the 17 samples does not reveal any specific age-related clustering. **(C)** Meta-gene plot across age groups demonstrates a similar pattern.